# Super-resolution optical microscopy study of telomere structure

Mary Lisa Phipps
Peter M. Goodwin
Jennifer S. Martinez
Edwin H. Goodwin

# Super-resolution optical microscopy study of telomere structure

Mary Lisa Phipps,[a] Peter M. Goodwin,[a] Jennifer S. Martinez,[a,b] and Edwin H. Goodwin[c,*]
aLos Alamos National Laboratory, Center for Integrated Nanotechnologies, P.O. Box 1663, Bikini Atoll Road, SM-30, Los Alamos, New Mexico 84545, United States
bLos Alamos National Laboratory, Institute for Materials Science, P.O. Box 1663, Bikini Atoll Road, SM-30, Los Alamos, New Mexico 84545, United States
cThe New Mexico Consortium, 100 Entrada Drive, Los Alamos, New Mexico 87544, United States

**Abstract.** Chromosome ends are shielded from exonucleolytic attack and inappropriate end-joining by terminal structures called telomeres; these structures are potential targets for anticancer drugs. Telomeres are composed of a simple DNA sequence (5′-TTAGGG-3′ in humans) repeated more than a thousand times, a short 3′ single-stranded overhang, and numerous proteins. Electron microscopy has shown that the 3′ overhang pairs with the complementary strand at an internal site creating a small displacement loop and a large double-stranded "t-loop." Our goal is to determine whether all telomeres adopt the t-loop configuration, or whether there are two or more distinct configurations. Progress in optimizing super-resolution (SR) microscopy for this ongoing investigation is reported here. Results suggest that under certain conditions sample preparation procedures may disrupt chromatin by causing loss of nucleosomes. This finding may limit the use of SR microscopy in telomere studies. © 2016 Society of Photo-Optical Instrumentation Engineers (SPIE) [DOI: 10.1117/1.JBO.21.9.094003]

## 1 Introduction

Even before the structure of DNA was known, Muller[1] and McClintock[2] realized natural chromosome ends must be shielded from end-joining reactions. We now know eukaryotic genomes are composed of double-stranded linear DNA molecules and that these ends are susceptible to exonucleolytic attack and incomplete replication in addition to inappropriate end-joining by DNA double-strand break repair enzymes, the problem identified by Muller and McClintock. Muller named the hypothesized shield the "telomere," Latin for "end part," in reference to its terminal location on the chromosome. In vertebrates, telomeres are complex structures composed of a simple double-stranded DNA sequence (5′-TTAGGG-3′) repeated more than a thousand times and ending in a short 3′ overhang. A six-protein complex called shelterin binds telomere DNA and several other proteins engage telomeres transiently.[3] The importance of telomeres in maintaining chromosomal stability is seen most dramatically when severe telomere dysfunction is induced experimentally by interfering with the actions of the shelterin proteins or other accessory proteins required to create functional telomeres. In such cases, chromosomes fuse end-to-end into long concatenates.[4] Less severe telomere dysfunction results in cell death, cellular senescence that drives the aging process, or initiation of a mutagenic process that may lead to cancer. Thus, telomeres are an essential component in maintaining stable transmission of genetic information; detailed understanding of how they perform this function is the subject of intense investigation.

The telomeres of many species form a large loop (t-loop) in which a short 3′ single-stranded overhang pairs with the complementary strand at an internal site creating a small displacement loop.[5] In addition to electron microscopy, t-loops have also been visualized with atomic force microscopy[6] and most recently with super-resolution (SR) optical microscopy.[7] The telomere t-loop configuration has been proposed to be an architectural solution to the problem of chromosome end protection in mammals and many other organisms. However, none of the imaging modalities have found t-loops on more than a minority of telomeric DNA fragments.[5–7] Despite reasonable explanations—nontelomere DNA contaminating samples, loss of loops during sample preparation, limited resolution, loops that fail to spread, and so on—these observations are also consistent with the hypothesis that t-loops are present on only a fraction of telomeres.

Although t-loops are a simple, elegant, and eminently plausible solution to the chromosome end problem, other structures have been proposed or observed in some organisms. Examples include G-quadruplexes, hairpin loops, end-binding proteins, and repetitive nontelomere DNA sequences, such as transposons.[8–12] Our own studies are motivated by a desire to understand the structural basis of chromosome end protection. In particular, we are trying to answer the question: Are t-loops a universal feature of all mammalian telomeres? We chose SR imaging in part due to the relative ease of sample preparation, and also because it was thought to better preserve the chromatin (DNA plus protein) structure of telomeres. SR microscopy is relatively new in telomere studies. The preparation and imaging of telomeres by SR microscopy, and interpretation of these images, are still evolving. Here, we report our progress in optimizing SR imaging for telomere studies.

*Address all correspondence to: Edwin H. Goodwin, E-mail: eds_mail2@msn.com

## 2 Experimental Methods

### 2.1 Surface Modification of Glass Coverslips

Borosilicate coverslips ($22 \times 22$-mm square, 0.18-mm thick, refractive index $n_D = 1.52$) were prepared for nuclei deposition using various methods: soaking in Alconox detergent (10% in water, 2 h), sonication in 1 M KOH for 15 min followed by extensive rinsing with nanopure water and drying under a stream of nitrogen, or plasma cleaning (Harrick PDC-32G, 5 min).

### 2.2 Mouse Embryonic Fibroblast Nuclei Preparation

Embryonic mouse fibroblasts (kindly provided by M. A. Kadhim, Oxford Brookes University, UK) were cultured in Dulbecco's Modified Eagle Medium supplemented with 10% fetal bovine serum, 1% penicillin/streptomycin, and 1% L-glutamine. Nuclei were prepared by harvesting approximately one hundred million mouse embryonic fibroblast (MEF) cells and osmotically shocking them in fibroblast lysis buffer (12.5 mM Tris pH 7.4, 5 mM KCl, 0.1 mM spermine, 0.25 mM spermidine, 175 mM sucrose). Cell outer membranes were lysed by incubation in 0.2% Nonidet-P40. Nuclei were crosslinked using 100 $\mu$g/ml psoralen (Trioxalen, Sigma). Nuclei were then lysed in spreading buffer (10 mM Tris pH 7.4, 10 mM ethylenediamine tetra-acetic acid, 0.05% sodium dodecyl sulfate, 1M NaCl, warmed to 37°C). Lysed nuclei solution containing ~70,000 nuclei was then deposited immediately onto cleaned coverslips. The deposition methods included dropcasting or spin-coating at various speeds (Plas-Labs/Headway Research PWM32; 250, 500, 750, and 1000 rpm with a distance from the center of rotation to the edge of the coverslip of ~10 mm), followed by evaporation, then fixing in methanol (−20°C, 10 min), and then acetone (−20°C, 1 min), followed by dehydration with stepwise ethanol rinses (70%, 95%, and 100% ethanol).

### 2.3 Fluorescence In situ Hybridization

MEF-fixed coverslips were rehydrated in phosphate-buffered saline and the sample side placed down on a glass microscope slide with 35 $\mu$l of hybridization buffer: 0.1 $\mu$M peptide nucleic acid (PNA)-Cy5 probe (PNA Bio Inc., Cy5 -5′-CCCTAACCCTAACCCTAA-3′), 70% formamide, 0.5% blocking reagent (Roche, part # 11096176001), and 10 mM Tris pH 7.2. The hybridization chamber was incubated at 80°C in 100% humidity for 10 min and allowed to cool slowly to room temperature overnight in a humid box in the dark. Coverslips were removed from the hybridization chamber and rinsed twice with 70% formamide, 10 mM Tris pH 7.2, followed by three rinses with 100 mM Tris pH 7.2, 150 mM NaCl, and 0.08% Tween-20. Coverslips were dehydrated stepwise with 70%, 95%, and 100% ethanol and stored in the dark for imaging.

### 2.4 Preparation of Hybridized Coverslips for Stochastic Optical Reconstruction Microscopy Imaging

Imaging chambers were prepared with hybridized coverslips by placing the coverslips sample-side down onto glass slides (Fisher 12-544-1) and sealing two sides with double-sided tape (80-$\mu$m thickness, 3 M). The oxygen-scavenging imaging buffer (50 mM Tris pH 8, 10 mM NaCl, 10% glucose, 100 mM beta-mercaptoethanol, 40 $\mu$g/ml catalase, 300 $\mu$g/ml glucose oxidase) was prepared immediately before use and added to the imaging chamber. The chamber was then sealed on the other two sides with nail polish.

### 2.5 Direct Stochastic Optical Reconstruction Microscopy

Direct stochastic optical reconstruction microscopy (dSTORM) was used to acquire SR images of telomeres labeled with the PNA-Cy5 hybridization probe. dSTORM is a single-molecule localization microscopy (SMLM) variant able to reconstruct an SR (subdiffraction limit) optical image from stacks of diffraction-limited images of individual, spatially isolated organic fluorophore labels (in this case Cy5).[13] Subdiffraction resolution is obtained by reconstructing the image from the centroid positions of the individual fluorophores that can be determined with a precision well below the diffraction limit. In SMLM, the areal density of the emitting labels must be limited so that the individual fluorophores are well resolved at the diffraction limit. With dSTORM, the label is photoswitched between long-lived dark and fluorescent states. With Cy5 this is done using a reducing buffer that reacts with the fluorophore in its triplet state (accessed by intersystem crossing from the first excited singlet state following 637-nm excitation of the singlet ground state) to form a long-lived dark (nonfluorescent) anionic radical. The dark anionic radical has an absorption near 400 nm that is used to return it to its neutral ground singlet state.[14]

The optical schematic of the imaging setup is shown in Fig. 1. Imaging of the PNA-Cy5-labeled telomeres was performed using this setup as described in detail elsewhere.[15] The setup consisted of an inverted microscope (Olympus IX-71) modified for through-objective total-internal-reflection evanescent-wave excitation and activation at 637 and 405 nm, respectively. Incidence angles were greater than the critical angle (~61 deg). The precise angle was not recorded but was chosen to optimize the signal-to-noise ratio in the image. The excitation beam was homogenized by expansion of the Gaussian excitation laser beam with a telescope and isolation of the central part of this using an iris. No corrections were made for under- and over-critical angle contributions to the images. The evanescent-wave excitation extended only ~100 nm into the aqueous buffer substantially reducing the fluorescence background from the
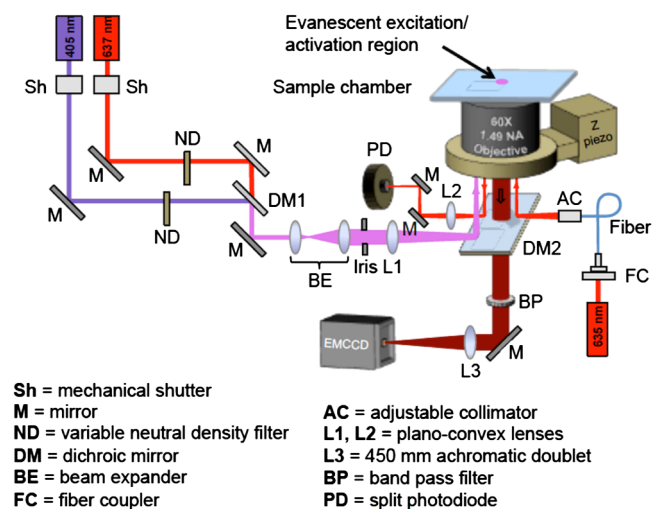


**Fig. 1** Optical schematic of the setup used for dSTORM imaging of Cy5-PNA-labeled telomeres.

imaging buffer. Cy5 fluorescence emission was collected by the same objective (Olympus APON OTIRF, ×60 1.49 NA), isolated from the scattered excitation light using a 37-nm wide bandpass filter centered at 676 nm (Semrock) and imaged onto an electron-multiplying CCD camera (Princeton Instruments) through the left-hand camera port of the modified inverted microscope base. The camera was used at an electron-multiplying gain setting of 50. Focus (z) drift during image acquisition was reduced using a focus-lock system.

The diameters of the overlapped 405-nm activation and 635-nm excitation regions at the cover glass/buffer interface were ~50 $\mu$m. Activation and excitation powers were 2 and 4.5 mW, respectively. Computer-controlled shutters in the activation and excitation beam paths were used to control these beams during the activation and excitation (imaging) cycles. Image stacks were collected in groups of 25 successive 100-ms exposure images between activation cycles. To control the areal density of activated (fluorescent) Cy5 labels and to accommodate irreversible photobleaching of the Cy5 labels during the course of image acquisition, the activation time was increased exponentially as a function of cycle number from 50 ms at cycle 1 to ~2500 ms at cycle 80. Stacks consisting of ~1000 to 2000 images (40 to 80 cycles) were collected from each of the examined regions of the samples. Under the excitation conditions used, spots due to single Cy5 molecule fluorescence were comprised of ~100 detected photons per 100 ms frame. The image stacks were analyzed using the DAOSTORM algorithm designed for spot localization in high spot density images.[16] We used the ImageJ plugin, ThunderStorm,[17] to reconstruct SR images from the DAOSTORM output (spot centroid $x - y$ positions and intensities). Lateral stage drift was corrected in ThunderStorm by cross-correlation of successive SR images reconstructed from successive substacks comprising an entire image stack. Lateral stage drifts during image acquisition were slowly varying and typically less than one camera pixel (106 nm) in $x$ and $y$. We chose to divide our data sets into five bins to capture the slow drift while maintaining good image statistics for the image cross-correlation drift-correction incorporated in Thunderstorm. YOYO-stained SR images of total DNA are shown in Fig. 2. PNA probe-stained telomere
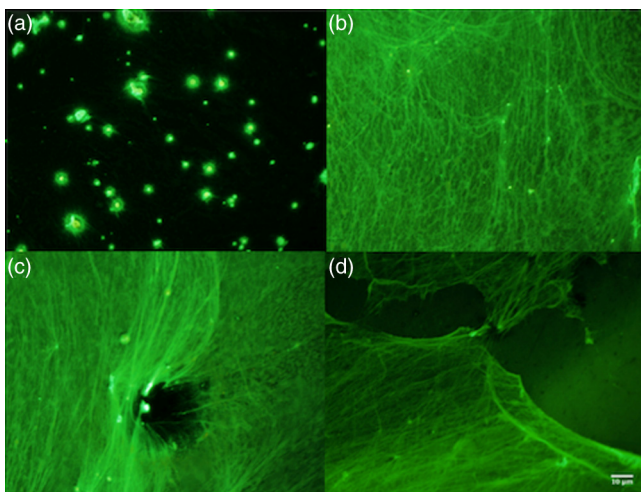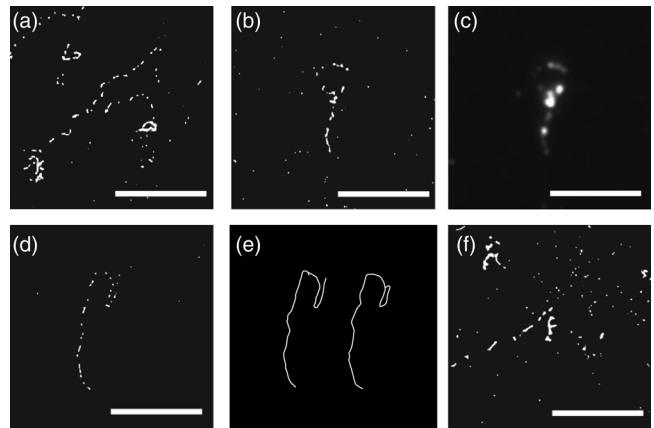


**Fig. 3** Classifying telomere morphology. Images of t-loops, and telomere fibers presumed to be t-loops, were obtained by dSTORM and placed into categories based on morphological characteristics. Scale bars are 5 $\mu$m. (a) Small compact loops with few or no gaps. Fiber continuity allows confidence in scoring members of this group as t-loops. (b) Extended loops with numerous gaps. These structures can be scored as t-loops, although with lesser confidence than compact loops, because a chance arrangement of telomere fragments into a well-structured loop would be highly improbable. (c) Diffraction-limited image of the t-loop in panel b. (d and e) Ambiguous "loops" and diagram of alternative interpretations (open versus closed). This group has the general appearance of loops often with breaks in which one or more fragments have been displaced. Confidence in scoring these structures as t-loops is low. (f) Y-shaped structures. The only branch point in a telomere fiber occurs at the stem-loop junction of a t-loop. Therefore Y structures are likely to be broken loops. However, the chance contact between two linear fragments cannot be ruled out, and therefore, Y structures cannot be scored confidently as t-loops.

fiber images are shown in Fig. 3. The full-width at half maximum of the point-spread function was 420 nm.

## 3 Results

### 3.1 Coverslip Cleaning Method

Testing of coverslip cleaning methods demonstrated that sonication in 1 M KOH yielded the best (cleanest and least autofluorescent as visualized microscopically) hydrophilic surface compared to plasma cleaning or Alconox soaking.

### 3.2 Sample Deposition

Deposition methods on coverslips included dropcasting or spin-coating at 250, 500, 750, and 1000 rpm. Neither dropcasting nor spin-coating at 250 rpm was enough to spread the DNA, while both 750 and 1000 rpm appeared to overstretch and tear telomere fibers. Coverslips coated at 500 rpm yielded fibers that did not show signs of damage when YOYO-stained and observed microscopically (Fig. 2).

### 3.3 Evaluation of Telomere Fiber Images.

Nuclei extracted from MEF cells were deposited onto coverslips at 500 rpm and stained with a PNA telomere probe. In contrast to YOYO1, a general DNA stain, the PNA probe is highly specific to telomere DNA allowing telomeres to be visualized



**Fig. 2** YOYO1-stained mouse MEF nuclei deposited at various spin-casting speeds. (a) 250, (b) 500, (c) 750, and (d) 1000 rpm.

against an ~1500-fold excess of nontelomeric DNA. Imaging by dSTORM revealed both t-loops and linear fibers, and each showed a wide range of spreading. There were smaller, compact structures and larger, stretched out structures. Few t-loops consisted of a continuous fiber, free of apparent gaps or breaks. In general the more stretched a structure, the more discontinuities it had. Examples of t-loops with different degrees of spreading are shown in Fig. 3.

We classified t-loops into four groups according to degree of spreading and continuity of the fiber. The four groups are (1) small compact loops with few or no gaps [Fig. 3(a)], (2) loops with greater spreading and more numerous gaps [Fig. 3(b)], (3) ambiguous "loops" [Fig. 3(d)], and (4) Y-shaped structures that may be broken loops [Fig. 3(f)]. The first group contained the most convincing examples of t-loops. Members of the last three groups all contained discontinuities, and, therefore, categorization as a loop is somewhat subjective.

## 4 Discussion

Estimates of the average size of an MEF telomere vary greatly depending on factors such as cell line and method of measurement. In the example below, we will assume 25 kb is an average telomere length. The spacing between adjacent bases along the length of the double helix is 0.34 nm implying that a 25-kb telomere would be 8500-nm or 8.5-$\mu$m long. Chromatin is composed of DNA wrapped around nucleosomes, and this wrapping reduces the length of chromatin fibers by sevenfold leading to the expectation that an average-sized 25-kb telomere would be about 1.2 $\mu$m. Comparing to the scale bars, the average telomere imaged in our experiments is substantially longer than 1.2 $\mu$m, indicating that t-loops in classes 2, 3, and 4 are being stretched well beyond the natural length of chromatin fibers.

According to Marko and Siggia,[18] histones are released from DNA by a comparatively small force of 2 pN that would allow an average telomere to extend to 8.5 $\mu$m, the length of the DNA double helix. A stretching force of 50 pN overcomes stacking forces between adjacent bases, and the DNA molecule extends an additional 1.85-fold (to 15.7 $\mu$m for a 25-kb telomere). At ~600 pN, the covalent bonds in the DNA backbone break, and in our experiments, the individual fragments would move independently guided by local hydrodynamic forces until they contact and bind to the coverslip. With these facts in mind, we interpret the images as follows.

When sample deposition is done at 500 rpm, most of the structures we saw, whether looped or linear, had numerous gaps consistent with having experienced forces sufficient to cause loss of nucleosomes, as well as unstacking and breakage of DNA. The many small telomere pieces scattered around the images suggest breakage is common. Both compact and overspread telomeres can be seen in the same image. Therefore, the forces that spread chromatin must vary considerably in magnitude over short distances. Many of the telomeres shown by Doksani et al.[7] also appear to be overspread. Calculating from their data, the degree of compaction is 1.2-fold, close to the 1.0 expected for a naked double helix, and not the sevenfold compaction expected of DNA wound around nucleosomes. This is consistent with our results suggesting frequent loss of nucleosomes during spreading. Shelterin proteins have been shown to be at least partly responsible for compaction of telomeres.[19] Spreading forces sufficient to cause loss

of nucleosomal proteins may be strong enough to remove shelterin proteins as well.

The smaller stem-loop structures on the coverslips have few gaps or breaks and their length suggests they retain a nucleosomal structure. These smaller loops are clearly resolved by dSTORM and there is less ambiguity in scoring t-loops in compact structures with few breaks. Importantly overspread telomeres, having lost nucleosomes and most likely shelterin as well, will be unsuitable for studies of the native state of telomeric chromatin. All of these factors weigh in favor of minimizing overspreading as a goal of telomere sample preparation.

## References

1. H. J. Muller "An analysis of the process of structural changes in chromosomes of Drosophila," *J. Genet.* **40**, 1–66 (1940).
2. B. McClintock, "The stability of broken ends of chromosomes in Zea mays," *Genetics* **26**, 234–282 (1941).
3. R. Diotti and D. Loayza, "Shelterin complex and associated factors at human telomeres," *Nucleus* **2**, 119–135 (2011).
4. S. M. Bailey et al., "The kinase activity of DNA-PK is required to protect mammalian telomeres," *DNA Repair* **3**, 225–233 (2004).
5. J. D. Griffith et al., "Mammalian telomeres end in a large duplex loop," *Cell* **97**, 503–514 (1999).
6. A. Chen et al., "Direct visualization of telomeric DNA loops in cells by AFM," *Surf. Interface Anal.* **32**, 32–37 (2001).
7. Y. Doksani et al., "Super-resolution fluorescence imaging of telomeres reveals TRF2-dependent T-loop formation," *Cell* **155**, 345–356 (2013).
8. M.-J. Giraud-Panis et al., "One identity or more for telomeres," *Front. Oncol.* **3**, 48 (2013).
9. A. J. Cesare and J. Karlseder, "A three-state model of telomere control over human proliferative boundaries," *Curr. Opin. Cell Biol.* **24**, 731–738 (2012).
10. G. N. Parkinson, M. P. Lee, and S. Neidle, "Crystal structure of parallel quadruplexes from human telomeric DNA," *Nature* **417**, 876–880 (2002).
11. K.-H. Choi and B.-S. Choi "Formation of a hairpin structure by telomere 3′ overhang," *BBA* **1217**, 341–344 (1994).
12. M. P. Horvath et al., "Crystal structure of the Oxytricha nova telomere end binding protein complexed with single strand DNA," *Cell* **95**, 963–974 (1998).
13. M. Heilemann et al., "Subdiffraction-resolution fluorescence imaging with conventional fluorescent probes," *Angew. Chem. Int. Ed.* **47**, 6172–6176 (2008).
14. S. van de Linde et al., "Direct stochastic optical reconstruction microscopy with standard fluorescent probes," *Nat. Protoc.* **6**, 991–1009 (2011).
15. J. J. Han et al., "Actin restructuring during Salmonella typhimurium infection investigated by confocal and super-resolution microscopy," *J. Biomed. Opt.* **19**, 016011 (2014).
16. S. J. Holden, S. Uphoff, and A. N. Kapanidis, "DAOSTORM: an algorithm for high-density super-resolution microscopy," *Nat. Methods* **8**, 279–280 (2011).
17. M. Ovesný et al., "ThunderSTORM: a comprehensive ImageJ plug-in for PALM and STORM data analysis and super-resolution imaging," *Bioinformatics* **30**, 2389–2390 (2014).
18. J. F. Marko and E. D. Siggia, "Stretching DNA," *Macromolecules* **28**, 8759–8770 (1995).

19. J. N. Bandaria et al., "Shelterin protects chromosome ends by compacting telomeric chromatin," *Cell* **164**, 735–746 (2016).

**Mary Lisa Phipps** received her Bachelor of Arts from Colby College in biology, a Bachelor of Fine Arts from Massachusetts College of Art, and a Master of Fine Arts from San Francisco Art Institute. After a successful career within industrial biotechnology, she joined the Center for Integrated Nanotechnologies at Los Alamos National Laboratory in 2006.

**Peter M. Goodwin** received his BS degree in physics from the California Institute of Technology in 1980 and a PhD in applied and engineering physics from Cornell University in 1989. He held postdoctoral positions at the IBM Technology Laboratory, Endicott, New York, and at Los Alamos National Laboratory, Los Alamos, New Mexico. He has been a technical staff member at Los Alamos National Laboratory since 1993.

**Jennifer S. Martinez** received her BS in chemistry from the University of Utah and her PhD in bioinorganic chemistry in 2002 from the University of California Santa Barbara. After receiving a director's postdoctoral fellowship, she joined the technical staff in the Center for Integrated Nanotechnologies at Los Alamos National Laboratory.

**Edwin H. Goodwin** received his BS and MS degrees in physics from Fairleigh Dickinson University in 1971 and 1977, respectively. He received his PhD in biophysics from the University of California, Berkeley in 1988. After holding postdoctoral and technical staff member positions at Los Alamos National Laboratory from 1989 to 2006, he moved to Colorado to become one of five founders of KromaTiD Inc., a biotech company in Fort Collins.